Core Losses under DC Bias Condition based on Steinmetz Parameters

J. Mühlethaler*, J. Biela*, J. W. Kolar*, and A. Ecklebe†
*Power Electronic Systems Laboratory, ETH Zurich, Email: muehlethaler@lem.ee.ethz.ch
†ABB Switzerland Ltd., Corporate Research, CH-5405 Baden-Dättwil

***Abstract*—When designing inductive components, calculating core losses is a difficult and not yet entirely solved problem. In particular it is impossible to predict the influence of a DC premagnetization on the losses without performing extensive measurements. For this work, different materials have been tested to gain information how core losses are influenced by a premagnetization. Measurements on molypermalloy powder, silicon steel, nanocrystalline material, and ferrite cores have been performed. Of the tested materials, a premagnetization mainly influences losses in ferrites and nanocrystalline materials, whereas the influence of a premagnetization in molypermalloy powder cores, and cores of silicon steel is negligible. The *Steinmetz Premagnetization Graph* (SPG) that shows the dependency of the Steinmetz parameters (α, β and k) on premagnetization is introduced. This permits the calculation of core losses under DC bias conditions. Such graphs are given for different materials and different operating temperatures. In addition, a detailed description of the test system is given, as high accuracy is crucial.**

***Index Terms*—Core losses, ferrite, Steinmetz, DC bias.**

I. Introduction

When designing power electronic systems, predicting core losses is a difficult, and not yet entirely solved problem. Particularly, the influence of a DC bias on the losses is not entirely clarified. The most used equation that characterizes core losses is the power equation [1]

$$P_\mathrm{v} = k f^\alpha \hat{B}^\beta \tag{1}$$

where $\hat{B}$ is the peak induction of a sinusoidal excitation with frequency f, P_v is the time-average power loss per unit volume, and k, α, β are material parameters. The equation is often referred to as the Steinmetz equation, named after Charles P. Steinmetz, who proposed a similar equation, without the frequency dependence, in 1892 [2]. The material parameters k, α, and β are accordingly referred to as the Steinmetz parameters. They are valid for a limited frequency and flux density range. Unfortunately, the Steinmetz equation is only valid for sinusoidal excitation. This is a huge drawback, because in power electronics applications the material is mostly exposed to nonsinusoidal flux waveforms.

To overcome this limitation, and determine losses for a wider variety of waveforms, different approaches have been developed. A common method to determine core losses is to break up the loss into hysteresis loss P_h, classical eddy current loss P_cl, and "excess loss" P_exc [3], [4]

$$P_\mathrm{v} = P_\mathrm{h} + P_\mathrm{cl} + P_\mathrm{exc} \tag{2}$$

The approach of loss separation has a practical disadvantage: such models are based on parameters, which are not always available and difficult to extract. Hence, simpler models are desired.

Another approach to overcome the limitation of the Steinmetz equation is derived in [5], [6], and [7]. The analysis in [5] is motivated by the fact that the loss due to domain wall motion has a direct dependency of $\mathrm{d}B/\mathrm{d}t$. As a result, a modified Steinmetz equation is proposed. In [6] the approach is further improved and in [7] a method how to deal with minor hysteresis loops is presented and some minor changes on the equation are made. The approach of [5], [6], and [7] leads to the improved Generalized Steinmetz Equation (iGSE)

$$P_\mathrm{v} = \frac{1}{T}\int_0^T k_i \left|\frac{\mathrm{d}B}{\mathrm{d}t}\right|^\alpha (\Delta B)^{\beta-\alpha}\,\mathrm{d}t \tag{3}$$

where ΔB is peak-to-peak flux density and

$$k_i = \frac{k}{(2\pi)^{\alpha-1}\int_0^{2\pi}|\cos\theta|^\alpha 2^{\beta-\alpha}\mathrm{d}\theta}. \tag{4}$$

The parameters k, α, and β are the same parameters as used in the Steinmetz equation (1). The iGSE is capable of accurately calculating losses of any flux waveform, without requiring extra characterization of material parameters beyond the parameters for the Steinmetz equation. Nevertheless, the iGSE has a drawback: it neglects the fact that core losses vary under DC bias conditions, i.e. the Steinmetz parameters change under DC bias condition.

In many power electronics applications magnetic components are biased with a DC or low-frequency premagnetization, e.g. in Switched-Mode Power Supplies (SMPS). Within SMPS circuits, magnetic components that are operating under DC bias conditions are commonly used, and are often among the largest components. Many publications have shown, that the influence of DC bias on the material properties can not be neglected [8]–[13]. An approach how to handle DC bias losses is described in [14], [15] and [16]. There, losses are calculated with a loss map that is based on measurements. This loss map stores the loss information for many operating points, each described by the flux ripple ΔB, the frequency f, and a DC bias H_DC. It is explained, how this loss map can be used for calculating iron losses of inductors employed in power electronic systems. One parameter in the loss map is the DC premagnetization, thus the loss increase due to DC bias is considered in this approach. However, extensive measurements are necessary to build the loss

978-1-4244-5393-1/10/$26.00 ©2010 IEEE

map. In conclusion, any description of core losses under DC bias condition without extensive measurements is an unsolved problem.

This work proposes a new approach how to describe core losses under DC bias condition. A graph that shows the Steinmetz parameters' (α, β and k) dependency on premagnetization is introduced in Section IV. This enables the calculation of losses via the Steinmetz equation (1) or the iGSE (3) using appropriate Steinmetz parameters. A core loss measurement test setup has been built for this work and is presented in Section II. The accuracy of the system is analyzed in Section III.

II. Test setup to measure core losses

To perform measurements, the best measurement technique has to be selected first. In [17] different methods are compared. The B-H Loop Measurement has been evaluated as the most suitable. Amongst other advantages, this technique offers rapid measurement (compared to other methods, e.g. calorimetric measurement), copper losses are not measured, and a good accuracy. In Section III the accuracy is analyzed in detail. The principles are as follows: two windings are placed around the Core Under Test (CUT). The sense winding (secondary winding) voltage v is integrated to sense the core flux density B

$$B(t) = \frac{1}{N_2 \cdot A_\mathrm{e}} \int_0^t v(\tau)\mathrm{d}\tau \tag{5}$$

where N_2 is the number of sense winding turns and A_e the effective core cross section of the CUT. The current in the excitation winding (primary winding) is proportional to the magnetic field strengths H

$$H(t) = \frac{N_1 \cdot i(t)}{l_\mathrm{e}} \tag{6}$$

where N_1 is the number of excitation winding turns and l_e the effective magnetic path length of the CUT. The loss per unit volume is then the enclosed area of the B-H loop, multiplied by the frequency f[1]

$$\frac{P}{V} = f \oint H\mathrm{d}B. \tag{7}$$

The selected approach is widely used [7], [15]. The test system consists of an oscilloscope, a power supply, a heating chamber, and a power stage, as illustrated in Fig. 1. It is controlled by a MATLAB program running on the oscilloscope under Microsoft Windows. In Table I the used equipment is listed. In Fig. 2 a photograph **(a)** and the simplified schematic **(b)** of the power stage is shown. In Table II the most important components employed in the power stage are listed. The power stage is capable of a maximal input voltage of $450\,\mathrm{V}$, output current of $25\,\mathrm{A}$ and a switching frequency of up to $200\,\mathrm{kHz}$. With the power stage, it is possible to achieve a rectangular voltage shape across the CUT, that leads to a triangular current shape including a DC bias (if desired). This behavior is illustrated in Fig. 3. To control the DC current, the current is sensed by a DC current transducer. A low frequency sinusoidal excitation is also possible, for this an output filter has been designed to achieve a sinusoidal current/voltage shape for frequencies up to $1\,\mathrm{kHz}$.

[1]The core loss per unit volume is

$$\frac{P}{V} = \frac{f\int_0^T i_1(t)\frac{N_1}{N_2}v_2(t)\mathrm{d}t}{A_\mathrm{e}l_\mathrm{e}} = \frac{f\int_0^T H(t)l_\mathrm{e}\frac{1}{N_1}N_1A_\mathrm{e}\frac{\mathrm{d}B(t)}{\mathrm{d}t}\mathrm{d}t}{A_\mathrm{e}l_\mathrm{e}}$$
$$= f\int_{B(0)}^{B(T)} H(B)\,\mathrm{d}B = f\oint H\mathrm{d}B,$$

where $\frac{N_1}{N_2}v_2(t)$ is the sense winding voltage transformed to the primary side.

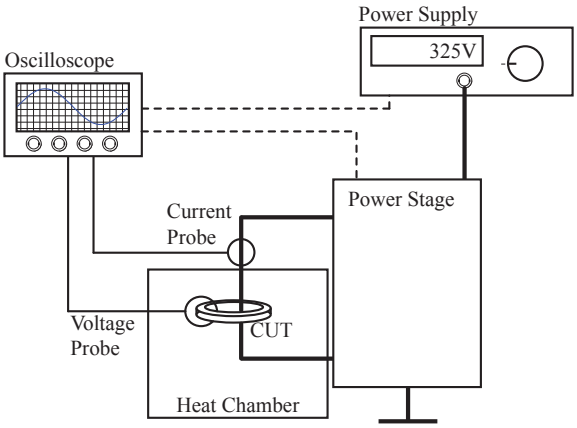

Fig. 1. Overview of the test system.

TABLE I
Measurement Equipment

Oscilloscope	LeCroy WaveSurfer 24MXs-A
Current Probe	LeCroy AP015
Heating Chamber	Binder ED53
Power Supply	Xantrex XTR 600-1.4
Power Stage	$0 - 450\,\mathrm{V}$ $0 - 25\,\mathrm{A}$ $0 - 200\,\mathrm{kHz}$

TABLE II
Power Stage Components

Power MOSFETs	IXYS IXFB82N60P
Gate Driver	IXYS IXDD414SI
Capacitors	Electrolytic: $2.75\,\mathrm{mF}$ Foil: $360\,\mu\mathrm{F}$ Ceramic: $3.86\,\mu\mathrm{F}$
DSP	TI TMS320F2808
Current Sensor	LEM LTS 25-NP
Fan	San Ace 40 GE

III. Accuracy of the Measurement System

The different aspects that influence the accuracy of the measurements are given in the following.

A. Phase Shift Error of Voltage and Current Measurement

According to [18], the error due to an inaccurate measurement of the voltage and current phase displacement can be quantified as

$$E = 100 \cdot \frac{\cos(\zeta + \phi) - \cos\zeta}{\cos\zeta}, \tag{8}$$

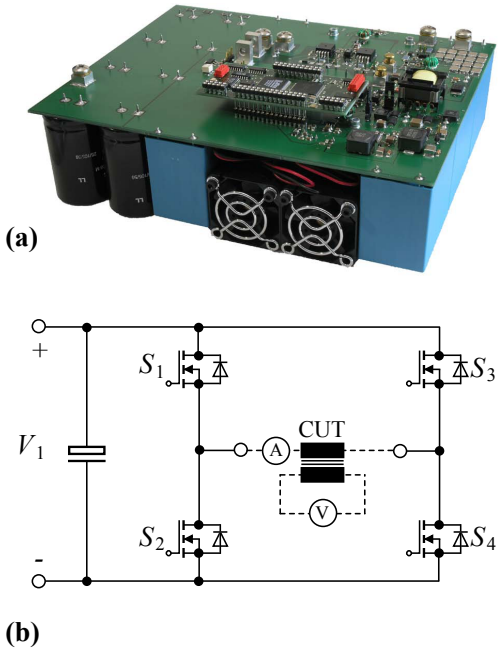

Fig. 2. Power stage **(a)** photograph, **(b)** simplified schematic.

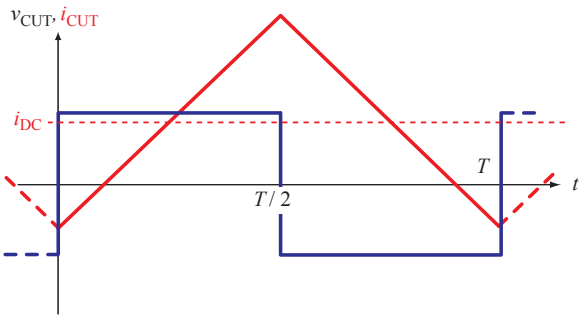

Fig. 3. Current and voltage waveforms of the CUT.

where E is the relative error in % of the measured core losses, ζ is the actual phase shift between the sense winding output voltage and the excitation winding current, and ϕ is the error in the measurement of ζ. Measurements have shown, that ϕ is linearly depending on the frequency. In other words, ϕ originates from a dead time T_d that is independent of the frequency. This dead time T_d can be measured with a rectangular current shape through a low inductance shunt, and with it the dead time can be compensated.

In Section IV measurements with the material ferrite N87 from EPCOS (core part number: B64290L22X87) are presented, therefore a short discussion about phase shift accuracy is given using the example of this core. In Fig. 4 a simplified equivalent circuit of the Core Under Test (CUT) is given. Winding losses and leakage inductance are assumed to be negligible. The reactance X_m can be calculated as

$$X_\mathrm{m} = \omega A_\mathrm{L} N_1^2, \tag{9}$$

where A_L is the inductance factor, N_1 is the number of primary winding turns, and $\omega = 2\pi f$ is the angular

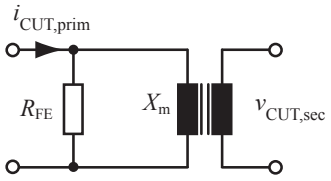

Fig. 4. Equivalent circuit of the CUT.

frequency. Hence, for the CUT ($A_\mathrm{L} = 2560\,\mathrm{nH}$ [19], $N_1 = 10$) and a frequency $f = 100\,\mathrm{kHz}$ the reactance is $X_\mathrm{m} = 160.8\,\Omega$. According to the material datasheet [19], at the operating point $\Delta B = 100\,\mathrm{mT}$, $f = 100\,\mathrm{kHz}$, and $T = 40\,^\circ\mathrm{C}$ losses of $P_\mathrm{Loss} = 0.2\,\mathrm{W}$ are expected. With this information, the equivalent resistor R_FE which represents the core losses can be calculated

$$R_\mathrm{FE} = \frac{V_\mathrm{rms}^2}{P_\mathrm{Loss}} = \frac{\left(N_1 A_\mathrm{e} \omega \frac{\Delta B}{2\sqrt{2}}\right)^2}{P_\mathrm{Loss}}, \tag{10}$$

where A_e is the equivalent core cross section. For the CUT and operating point, the resistor R_FE is $2.26\,\mathrm{k\Omega}$. Now, the angle ζ can be calculated as

$$\zeta = \arctan \frac{R_\mathrm{FE}}{X_\mathrm{m}} = 85.9\,^\circ \tag{11}$$

An uncompensated dead time T_d would result in a phase shift error of voltage and current measurement of

$$\phi = f \cdot T_\mathrm{d} \cdot 360\,^\circ. \tag{12}$$

Inserting (12) in (8), and solving for T_d, leads to a tolerable uncompensated dead time for a desired accuracy, e.g. for an accuracy of $\pm 3\,\%$, an uncompensated dead time of $\pm 3.5\,\mathrm{ns}$ at $100\,\mathrm{kHz}$ and $\zeta = 85.9\,^\circ$ would be tolerable. Measurements have shown, that the dead time compensation leads to lower residual dead times, although a quantification is difficult. Assuming a realistic dead time compensation to an accuracy of $\pm 1.5\,\mathrm{ns}$, and expecting a system accuracy (only phase shift consideration) of $\pm 4\,\%$, measurements of materials up to an angle of $\zeta = 88.7\,^\circ$ (at $f = 100\,\mathrm{kHz}$) can be performed. At lower frequency measurements the permitted angle ζ increases for the same accuracy constraint, e.g. at $20\,\mathrm{kHz}$, for an accuracy of $\pm 4\,\%$, measurements up to an angle of $\zeta = 89.7\,^\circ$ are permitted. All measurements presented in the next sections are within this range.

The system has one drawback related to the phase shift: measuring gapped cores (or low permeability cores) is difficult because the angle ζ substantially increases in this situation. A detailed analysis together with a new method of how gapped cores could be measured is introduced in [13]. However, for this work only un-gapped cores have been measured.

B. Equipment Accuracy

A typical magnitude/frequency characteristic of the current probe has been provided by the current probe manufacturer LeCroy, from which an AC accuracy of 3 % could be extracted. Together with the accuracy of

the passive probe (attenuation accuracy of 1 %), and the accuracy of the oscilloscope itself (1.5 %, that originates amongst others from the limited vertical resolution of 8 bit), an equipment accuracy of $\leq |\pm 5.6\,\%|$ is derived.

C. Capacitive Couplings

Capacitive currents may result in errors and must therefore be avoided. The typical capacitances that are present in windings are

- capacitance between the primary and secondary winding (inter capacitance),
- self capacitance between turns of a winding (intra capacitance),
- and capacitance between the windings and the magnetic core.

According to [20], the inter and intra capacitances increase when the core is grounded, thus the core should not be grounded. Generally, the inter and intra capacitances increase with increasing area between the windings and decrease with distance between the windings. To decrease the inter capacitance, separating the windings is favorable, although separating the windings avoids an absolute uniform winding distribution around the core (ideally, the primary winding should be distributed uniformly around the core to achieve a homogenous flux density distribution). Another important aspect of the winding arrangement is the chosen number of turns of the primary winding. Even with the use of favorable winding layout, some ringing in current and voltage is inevitable. Less turns are more favorable for two reasons: this additionally decreases parasitic capacitances, and, because the current for the same magnetic operating point is higher, capacitive currents are relatively lower compared to (desired) inductive currents.

D. Temperature

An important aspect for performing the measurement is that the temperature of the CUT is defined and constant. To keep the temperature constant, the test system performs the measurement automatically (starts excitation, controls current, regulates flux (ΔB), triggers the oscilloscope, reads values). With such an automated measurement system, a working point is rapidly measured and the losses do not heat the core in the short measurement period.

E. Comparative Measurement and Conclusion

Comparative measurements with the power analyzer *Norma D6100* have been performed to confirm the accuracy. The power analyzer is connected to measure the excitation winding current and the sense winding voltage to obtain core losses [17]. The results in the performed working points matched very well. The deviation between the results of the test system and of the power analyzer was always $\leq |\pm 4\,\%|$ (up to 100 kHz).

From the equipment accuracy ($\leq |\pm 5.6\,\%|$) and the phase shift accuracy ($\leq |\pm 4\,\%|$), a system accuracy of $\leq |\pm 9.8\,\%|$ is calculated. However, based on the results of the comparative measurements, it can be said that the reached accuracy is higher.

Concluding, a test system has been built up, that performs the measurements quickly and leads to sufficiently accurate results.

IV. Core Losses of Ferrites Under DC Bias Condition

In this section, measurement results are presented and a new approach to describe core losses under DC bias conditions is introduced, which is based on a graph that shows the dependency of the Steinmetz parameters (α, β and k) on premagnetization. This is done using the example of the material ferrite N87 from EPCOS (core part number B64290L22X87 [19]). In Fig. 5 the core losses and in Fig. 6 the core losses normalized to the losses P_0 at zero premagnetization are shown for different DC bias values. In Fig. 7 the losses are plotted in function of the frequency f, with and without DC bias. Describing losses via the Steinmetz equation (1) or the iGSE (3) is the most common method, hence improving this method would be most beneficial for design engineers. As the iGSE (3) is more suitable for describing core losses in power electronic applications, in all following considerations, the three discussed parameters are α, β, and k_i of the iGSE (α, β are the same as in (1), while k_i is described in (4)). For the applied waveform as illustrated in Fig. 3 (triangular current/flux shape), (3) leads to

$$P_\mathrm{v} = k_i (2f)^\alpha \Delta B^\beta. \tag{13}$$

When a core is under DC bias condition, the losses still can be described with the Steinmetz equation (1) or the iGSE (3), i.e. the losses still follow the power equation stated by Steinmetz. However, the Steinmetz parameters must be adjusted according to the DC bias present. As will be shown in the following, a DC bias causes changes in the Steinmetz parameters β and k_i, but not in the parameter α.

- The losses change when keeping ΔB and frequency f constant and varying the DC bias H_DC (cf. Fig. 5). Thus, the Steinmetz parameter k_i depends on the DC bias H_DC ($k_i = f(H_\mathrm{DC})$).

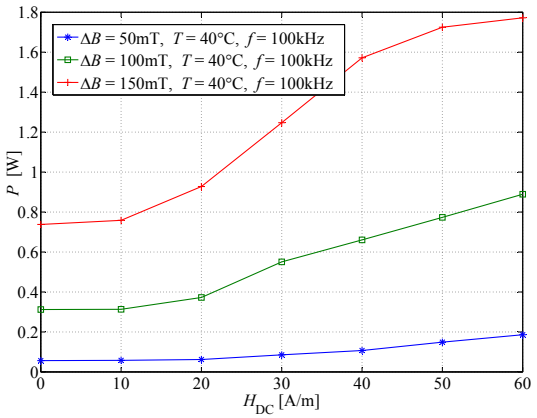

Fig. 5. Core losses under DC bias conditions (ferrite N87; measured on R42 core), $f = 100\,\mathrm{kHz}$, $T = 40\,^\circ\mathrm{C}$.

- Keeping the frequency f constant, the factor by which the losses increase due to a premagnetization H_{DC} differs for different ΔB (cf. Fig. 6). Thus, the Steinmetz parameter β depends on the premagnetization H_{DC} as well ($\beta = f(H_{\mathrm{DC}})$).

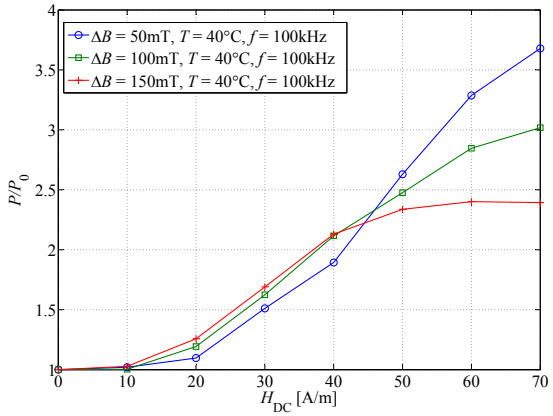

Fig. 6. Core losses under DC bias conditions, normalized to losses P_0 at zero premagnetization (ferrite N87; measured on R42 core), $f = 100\,\mathrm{kHz}$, $T = 40\,^{\circ}\mathrm{C}$.

- According to [8], the influence of a DC bias does not depend on the measurement frequency f. This has been confirmed. As can be seen in Fig. 7, at a constant ΔB, the factor by which the losses increase due to a premagnetization H_{DC} is the same for different frequencies f (the slopes of the curves remain the same). Hence, the Steinmetz parameter α is independent of the premagnetization H_{DC} ($\alpha = \mathrm{const.}$). The fact, that α is constant has been confirmed to frequencies up to $100\,\mathrm{kHz}$, no measurements above this frequency have been performed, hence no information can be given, whether and up to which frequency α is constant.

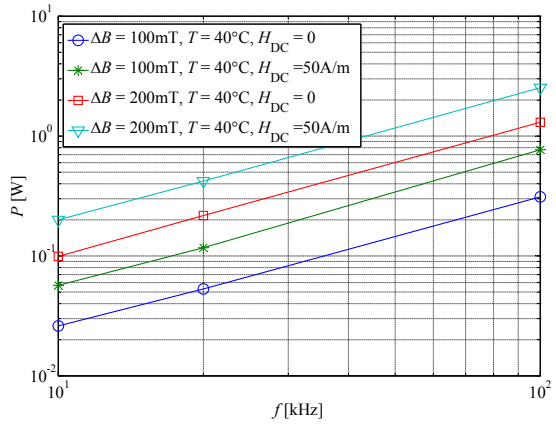

Fig. 7. Core losses (ferrite N87; measured on R42 core), $T = 40\,^{\circ}\mathrm{C}$.

For the material N87 from EPCOS the dependencies $\beta = f(H_{\mathrm{DC}})$ and $k_i = f(H_{\mathrm{DC}})$ are given in Fig. 8, and normalized to β_0 and k_{i0} in Fig. 9. β_0 and k_{i0} are the Steinmetz parameters at zero premagnetization. We call the graph illustrated in Fig. 9 the *Steinmetz Premagnetization Graph* (SPG). Its derivation is discussed

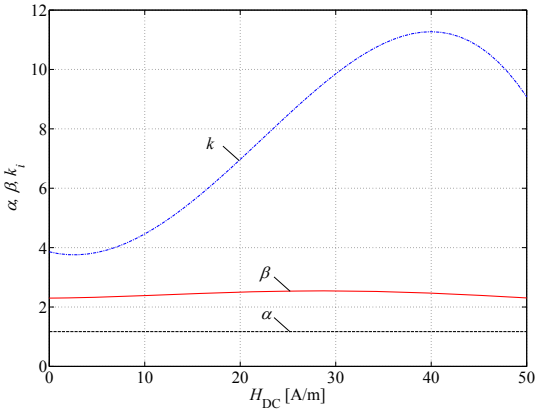

Fig. 8. Steinmetz parameters in function of premagnetization H_{DC} (ferrite N87), $T = 40\,^{\circ}\mathrm{C}$.

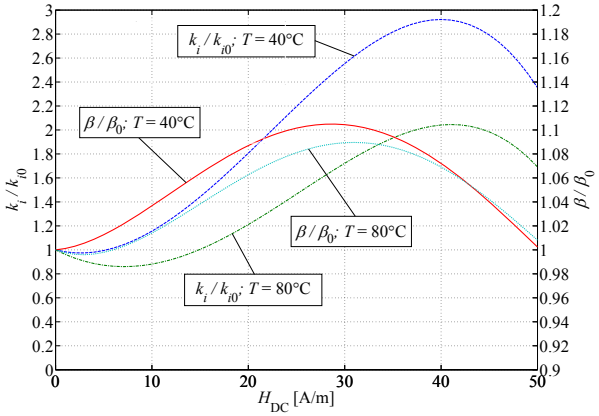

Fig. 9. SPG of the material ferrite N87 (EPCOS).

in Appendix A. The SPG is very useful and it would be valuable to have such a graph in the data sheet of a magnetic material as it would then be possible to calculate core losses under a DC bias condition. Fig. 10 shows how the measured and, based on the SPG, calculated curves compare. For the considered working points ($\Delta B = 50\,\mathrm{mT}/100\,\mathrm{mT}/150\,\mathrm{mT}$, $f = 20\,\mathrm{kHz}/100\,\mathrm{kHz}$) an error of $\leq |\pm 10\,\%|$ has been achieved. In Appendix B SPGs of other materials (Ferroxcube 3F3 (ferrite), EPCOS N27 (ferrite), and VAC VITROPERM 500F (nanocrystalline material)) are given. Furthermore, a discussion how to extract the Steinmetz parameter value k from the SPG is given in Appendix C.

V. Influence of Temperature

For an accurate core calculation, the temperature is another important parameter that considerably influences core losses. In Fig. 11 the losses normalized to losses P_0 at zero premagnetization are given for different temperatures. As can be seen, for the material ferrite N87, at higher temperatures the influence of a premagnetization to core losses reduces. The temperature influence is described by extending the SPG to curves of different operating temperatures, as is shown in Fig. 9.

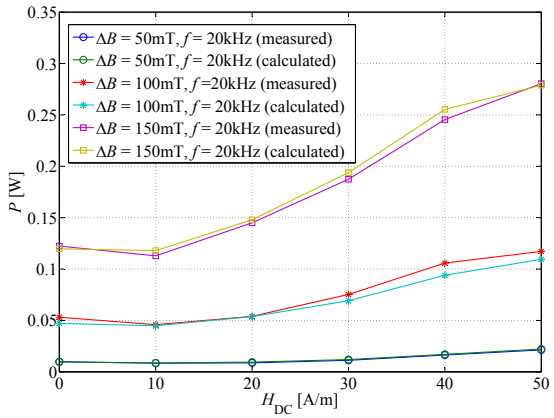

Fig. 10. Core losses under DC bias conditions: measured and calculated curves (ferrite N87), $f = 20\,\mathrm{kHz}$, $T = 40\,^\circ\mathrm{C}$.

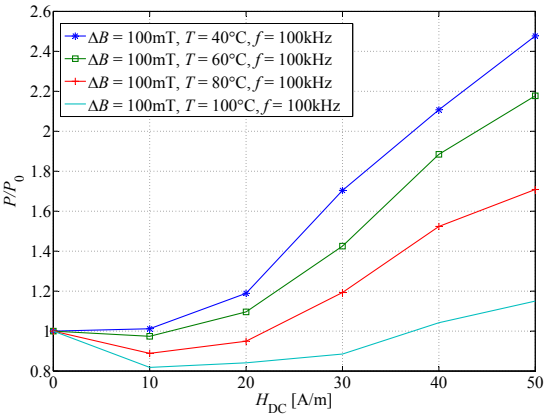

Fig. 11. Core losses under DC bias conditions: measured at different operating temperatures. Normalized to losses P_0 at zero premagnetization. Material N87.

VI. Example How to Use the SPG

In the previous sections, the SPG has been introduced. This section presents now an easy to follow example that illustrates how to calculate core losses of the inductor of a power electronics converter with help of the SPG. In Fig. 12 the schematic and the inductor current waveform of a buck converter, and in Table III the corresponding specifications are given. For the inductor L a DC bias of $H_{\mathrm{DC}} = 44\,\mathrm{A/m}$, and a flux density ripple of $\Delta B = 73\,\mathrm{mT}$ is calculated. The following steps lead to the core losses occurring in the inductor:

- For the used material, the corresponding Steinmetz parameters are extracted from the datasheet. This is done by solving (1) at three operating points for α, β, and k: $\alpha = 1.25$, $\beta = 2.46$, $k = 15.9$ (values for temperature $T = 40\,^\circ\mathrm{C}$, at zero premagnetization).
- Next, k_i is calculated according to (4): $k_i = 1.17$.
- k_i and β are now adjusted according to the SPG of the material N87 (cf. Fig. 9) for an operating point with $H_{\mathrm{DC}} = 44\,\mathrm{A/m}$: $k_i' = 2.8 \cdot k_i = 3.28$ and $\beta' = 1.04 \cdot \beta = 2.56$.
- Now, the losses are calculated according to (3). For piecewise linear waveforms, as is the case in the presented example, the integral of (3) may be split into one piece for each linear segment, so that a complicated numerical integration is avoided [7]. The losses follow as

$$\begin{aligned} P &= V_{\mathrm{e}} \frac{k_i'(\Delta B)^{\beta'-\alpha}}{T} \\ &\cdot \left(\left| \frac{\Delta B}{DT} \right|^{\alpha} DT + \left| \frac{\Delta B}{(1-D)T} \right|^{\alpha} (1-D)T \right) \\ &= V_{\mathrm{e}} \frac{k_i'(\Delta B)^{\beta'-\alpha}}{T} \\ &\cdot \left(\left| \frac{V_{\mathrm{in}} - V_{\mathrm{out}}}{N A_{\mathrm{e}}} \right|^{\alpha} DT + \left| \frac{-V_{\mathrm{out}}}{N A_{\mathrm{e}}} \right|^{\alpha} (1-D)T \right) \\ &= 52.8\,\mathrm{mW}, \end{aligned} \tag{14}$$

where $V_{\mathrm{e}} = 3079\,\mathrm{mm}^3$ is the effective core volume, $A_{\mathrm{e}} = 51.26\,\mathrm{mm}^2$ is the effective core cross section, $T = 1/f$ is the period length, and $D = 0.5$ is the duty cycle.

Assuming that the Steinmetz parameters had not been adjusted according to the SPG in the example above, the losses would have been calculated as $P = 24.5\,\mathrm{mW}$, which is an underestimation by a factor of more than two.

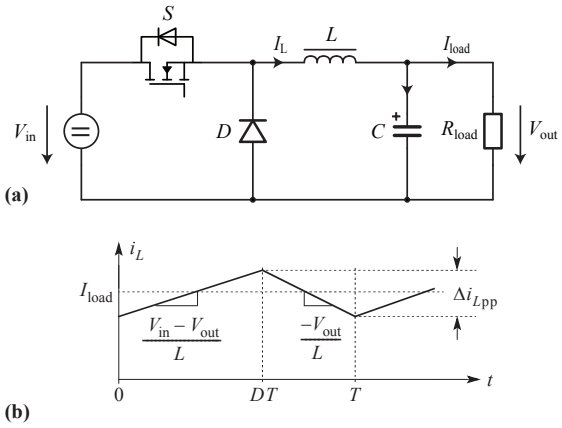

Fig. 12. Buck converter schematic **(a)** and current waveform **(b)** with specifications given in Table III.

TABLE III
Buck converter specifications.

V_{in} / V_{out}	12 V / 6 V
f	100 kHz
P	2 W
I_{load}	0.33 A
L	150 μH (EPCOS N87; R25; N=8) (core part number: B64290L618X87 [19])

VII. Core Losses Under DC Bias Condition of Different Materials

Different materials have been tested to gain information how core losses are influenced by a premagnetization in different materials. Measurements on a molypermalloy powder core (Magnetics MPP 300u) and cores of silicon steel (tested: ET165-35 grain-oriented steel with lamination thickness 0.35 mm, M470-50A non-oriented

steel with lamination thickness $0.5\,\mathrm{mm}$) have shown that the losses are unaffected (or change only very little) by a premagnetization. The measurements on the silicon steel cores have been performed up to a DC magnetic field strengths of $1400\,\mathrm{A/m}$ (core is already out of its linear region). For very high H_{DC}, a small loss increase has been observed (e.g. for steel M470-50A $25\,\%$ higher losses than at zero premagnetization have been observed at a DC magnetic field strengths of $1400\,\mathrm{A/m}$). The tested powder core (Magnetics MPP 300u; part number: C055433A2) has been tested up to a DC magnetic field strengths of $1200\,\mathrm{A/m}$, up to that operating point the loss change is negligible small.

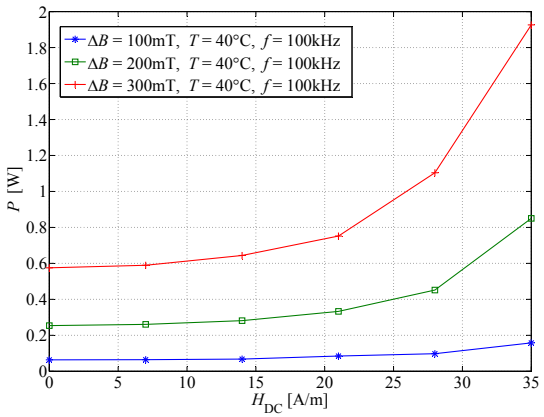

Fig. 13. Core losses under DC bias conditions; material VITROPERM 500F (VAC); core: W452; $f = 100\,\mathrm{kHz}$, $T = 40\,^{\circ}\mathrm{C}$.

TABLE IV
IMPACT OF DC BIAS TO CORE LOSSES, AN OVERVIEW OF DIFFERENT MATERIAL CLASSES.

Material Class	**Measured Material(s)**	**Impact on Losses?**
Soft Ferrites	EPCOS N87, N27, T35 Ferroxcube 3F3	yes
Nanocrystalline	VITROPERM 500F (VAC)	yes
Silicon Steel	M470-50A non-oriented steel ET165-35 grain-oriented steel	negligible
Molypermalloy Powder	Magnetics MPP300	negligible

Losses in the nanocrystalline material VITROPERM 500F from Vacuumschmelze increase under DC bias condition, as can be seen in Fig. 13. The SPGs of the material VITROPERM 500F and of some more ferrites are given in Appendix B. In Table IV an overview of the tested materials is given. Tests have been performed only on the above listed components, hence, a general declaration of the whole material class cannot be made with $100\,\%$ certainty.

VIII. Conclusion and Future Work

A graph that shows the dependency of the Steinmetz parameters (α, β and k) on premagnetization, i.e. the *Steinmetz Premagnetization Graph* (SPG) has been introduced. Based on the SPG, calculating core losses under DC bias condition becomes possible. It is shown, that the graph is independent of the frequency f, and therewith applicable for a wide frequency range. This new approach of describing losses under DC bias condition is promising due to its simplicity: only the SPG would have to be added to a magnetic material data sheet.

Appendix A
Derivation of the Steinmetz Premagnetization Graph

The Steinmetz parameters in function of H_{DC} are described with a fourth order series expansion

$$\begin{bmatrix}\alpha\\ \beta\\ k_i\end{bmatrix} = \begin{bmatrix}\alpha_0 & 0 & 0 & 0 & 0\\ \beta_0 & p_{\beta 1} & p_{\beta 2} & p_{\beta 3} & p_{\beta 4}\\ k_{i0} & p_{ki1} & p_{ki2} & p_{ki3} & p_{ki4}\end{bmatrix} \cdot \begin{bmatrix}1\\ H_{\mathrm{DC}}\\ H_{\mathrm{DC}}^2\\ H_{\mathrm{DC}}^3\\ H_{\mathrm{DC}}^4\end{bmatrix} \quad (15)$$

or

$$\mathbf{S} = \mathbf{P} \cdot \mathbf{H}. \quad (16)$$

To extract the dependency of the Steinmetz parameters on the premagnetization, one has to find the right coefficients of the matrix $\mathbf{P}$. This is an optimization problem. A least square algorithm has been implemented that fits measured curves with calculated data by minimizing the relative error at 3 different values of ΔB, each measured at two frequencies, and 6 premagnetization values H_{DC} (including $H_{\mathrm{DC}} = 0$). The losses are calculated according to (13) with Steinmetz parameters from (15)/(16). In the initial matrix $\mathbf{P}$, all elements p_* (cf. (15)) are set to zero. The values that represent the Steinmetz values under no DC bias condition (α_0, β_0, and k_{i0}) have reasonable initial values. As an optimization constraint, it is assumed that $\alpha(H_{\mathrm{DC}}) > 1$ and $\beta(H_{\mathrm{DC}}) > 2$ for all values of H_{DC}. The optimization is based on the MATLAB function `fminsearch()` that applies the Downhill-Simplex-Approach of Nelder and Mead [21]. This optimization procedure leads to graphs for the Steinmetz dependency as Fig. 8, or normalized to β_0 respectively k_{i0} to the SPG as e.g. shown in Fig. 9.

Appendix B
SPGs of Other Materials

In Fig. 14 the SPG is given for the material EPCOS N27, and in Fig. 15 for the material Ferroxcube 3F3. In Fig. 16 the SPG for the nanocrystalline material VITROPERM 500F from Vacuumschmelze (VAC) is depicted. The independency of the frequency has been confirmed for all materials ($\alpha = \mathrm{constant}$).

Appendix C
Classic Steinmetz Parameter k

A short discussion how to extract the Steinmetz parameter value k (not k_i) from the SPG is given in the following. According to (4), for k we have

$$\frac{k}{k_0} = \frac{k_i (2\pi)^{\alpha-1} \int_0^{2\pi} |\cos\theta|^{\alpha} 2^{\beta-\alpha} \mathrm{d}\theta}{k_{i0} (2\pi)^{\alpha-1} \int_0^{2\pi} |\cos\theta|^{\alpha} 2^{\beta_0-\alpha} \mathrm{d}\theta}, \quad (17)$$

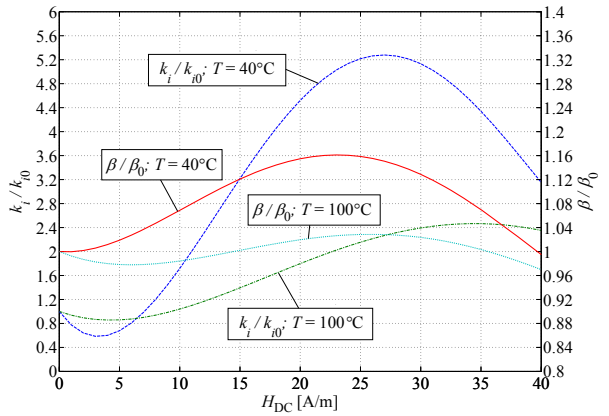

Fig. 14. SPG of the material ferrite N27 (EPCOS); measured on R25 core.

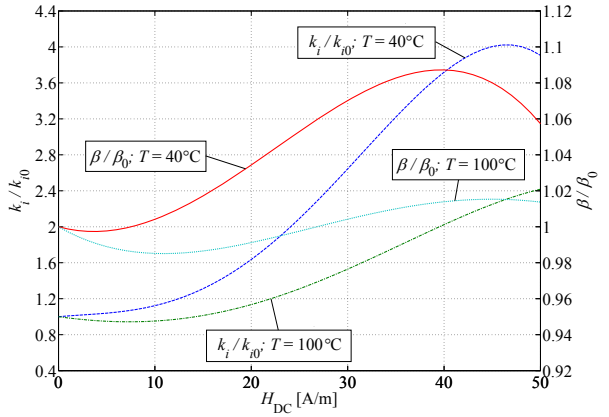

Fig. 15. SPG of the material ferrite 3F3 (Ferroxcube); measured on core type TN25/15/10.

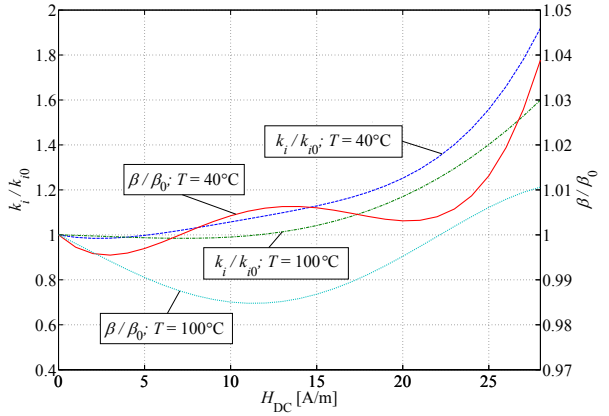

Fig. 16. SPG of the material VITROPERM 500F (VAC); measured on W452 core.

that is, assuming $\alpha = \text{constant}$,

$$\frac{k}{k_0} = \frac{k_i 2^{\beta}}{k_{i0} 2^{\beta_0}} = \frac{k_i}{k_{i0}} \cdot 2^{\left(\frac{\beta}{\beta_0}-1\right)\beta_0}, \qquad (18)$$

where $\frac{\beta}{\beta_0}$ can be extracted from the SPG. Of course, it is conceivable to write k/k_0 in the SPG, instead of k_i/k_{i0}. However, because the built test system excites the core with a triangular current shape, k_i/k_{i0} has been chosen for the graph. The iGSE is in any case very broadly used, hence, to avoid further calculations, directly having information about k_i is often desired.

REFERENCES

[1] E. C. Snelling, *Soft Ferrites, Properties and Applications*. 2nd edition, Butterworths, 1988.

[2] C. P. Steinmetz, "On the law of hysteresis," *Proceedings of the IEEE*, vol. 72, no. 2, pp. 197–221, 1984.

[3] G. Bertotti, *Hysteresis in Magnetism*. Academic Press, Inc., 1998.

[4] W. A. Roshen, "A practical, accurate and very general core loss model for nonsinusoidal waveforms," *IEEE Transactions on Power Electronics*, vol. 22, no. 1, pp. 30–40, 2007.

[5] J. Reinert, A. Brockmeyer, and R. De Doncker, "Calculation of losses in ferro- and ferrimagnetic materials based on the modified Steinmetz equation," *IEEE Transactions on Industry Applications*, vol. 37, no. 4, pp. 1055–1061, 2001.

[6] J. Li, T. Abdallah, and C. R. Sullivan, "Improved calculation of core loss with nonsinusoidal waveforms," in *Industry Applications Conference, 2001. 36th IEEE IAS Annual Meeting.*, vol. 4, pp. 2203–2210 vol.4, 2001.

[7] K. Venkatachalam, C. R. Sullivan, T. Abdallah, and H. Tacca, "Accurate prediction of ferrite core loss with nonsinusoidal waveforms using only Steinmetz parameters," in *Proc. of IEEE Workshop on Computers in Power Electronics*, pp. 36–41, 2002.

[8] G. Niedermeier and M. Esguerra, "Measurement of power losses with DC-bias - The Displacement Factor," in *Proc. of PCIM*, pp. 169–174, 2000.

[9] A. Brockmeyer, "Experimental evaluation of the influence of DC-premagnetization on the properties of power electronic ferrites," in *Proc. of the 11th Annual Applied Power Electronics Conference (APEC).*, vol. 1, pp. 454–460, 3–7 March 1996.

[10] T. Komma, *Allgemein gültiger Entwurfsalgorithmus für magnetische Komponenten in Schaltnetzteilen mit unterschiedlichen Topologien und Schaltfrequenzen bis 2 MHz*. PhD thesis, Technische Universität Dresden, 2005.

[11] M. S. Lancarotte, C. Goldemberg, and A. A. Penteado, "Estimation of FeSi core losses under PWM or DC bias ripple voltage excitations," *IEEE Transactions on Energy Conversion*, vol. 20, no. 2, pp. 367–372, 2005.

[12] C. A. Baguley, B. Carsten, and U. K. Madawala, "The effect of DC bias conditions on ferrite core losses," *IEEE Transactions on Magnetics*, vol. 44, pp. 246–252, Feb. 2008.

[13] C. A. Baguley, U. K. Madawala, and B. Carsten, "A new technique for measuring ferrite core loss under DC bias conditions," *IEEE Transactions on Magnetics*, vol. 44, no. 11, pp. 4127–4130, 2008.

[14] S. Iyasu, T. Shimizu, and K. Ishii, "A novel iron loss calculation method on power converters based on dynamic minor loop," in *Proc. of European Conference on Power Electronics and Applications*, pp. 2016 – 2022, 2005.

[15] T. Shimizu and K. Ishii, "An iron loss calculating method for AC filter inductors used on PWM inverters," in *Proc. of 37th IEEE Power Electronics Specialists Conference (PESC)*, pp. 1–7, 2006.

[16] K. Terashima, K. Wada, T. Shimizu, T. Nakazawa, K. Ishii, and Y. Hayashi, "Evaluation of the iron loss of an inductor based on dynamic minor characteristics," in *Proc. of European Conference on Power Electronics and Applications*, pp. 1–8, 2007.

[17] B. Carsten, "Why the magnetics designer should measure core loss; with a survey of loss measurement techniques and a low cost, high accuracy alternative," in *Proc. of PCIM*, pp. 163–179, 1995.

[18] V. Thottuvelil, T. Wilson, and J. Owen, H.A., "High-frequency measurement techniques for magnetic cores," *IEEE Transactions on Power Electronics*, vol. 5, pp. 41 –53, jan 1990.

[19] *Ferrites and Accessories, Edition 2007*. EPCOS AG.

[20] A. V. den Bossche and V. C. Valchev, *Inductors and Transformers for Power Electronics*. CRC Press, Taylor & Francis Group, 2005.

[21] J. A. Nelder and R. Mead, "A simplex method for function minimization," *The Computer Journal*, vol. 4, pp. 308–313, 1965.